AGU ADVANCING EARTH AND SPACE SCIENCE

Geophysical Research Letters

RESEARCH LETTER
10.1029/2020GL091345

Evolution of Subtropical Pacific-Onset El Niño: How Its Onset Location Controls Its Decay Evolution

Ji-Won Kim[1] and **Jin-Yi Yu**[1]

[1]Department of Earth System Science, University of California, Irvine, CA, USA

Key Points:

- The SP-onset El Niño has a larger uncertainty than the TP-onset El Niño in its decay evolution in both the observations and CESM1 simulation
- The onset location of SP-onset El Niño plays a critical role in controlling its decay evolution pattern
- The eastward (westward) onset event activates Indo-Pacific (tropical-subtropical Pacific) interactions, causing cyclic (multiyear) evolution

Supporting Information:

- Supporting Information S1

Correspondence to:
J.-W. Kim,
jiwok13@uci.edu

Citation:
Kim, J.-W., & Yu, J.-Y. (2021). Evolution of subtropical Pacific-onset El Niño: How its onset location controls its decay evolution. *Geophysical Research Letters*, *48*, e2020GL091345. https://doi.org/10.1029/2020GL091345

Received 21 OCT 2020
Accepted 23 JAN 2021

Abstract In the observations, El Niño events initiated by a subtropical Pacific mechanism (SP-onset El Niños) show larger uncertainty in their decay evolution patterns than those initiated by a tropical Pacific mechanism. A 2,200-year simulation of Community Earth System Model reproduces this observed feature and its SP-onset El Niños are analyzed to understand the cause of the large uncertainty. Results show that the onset location of SP-onset El Niño, which interacts with the eastern edge of the western Pacific warm pool, is a key factor controlling its decay evolution. When the onset is located east (west) of 155°E, the event has a strong tendency to reverse (maintain) its phase, leading to cyclic (multiyear) evolution. These two onset locations respectively activate Indo-Pacific and tropical-subtropical Pacific interactions to give rise to the different evolution patterns. The findings offer a potential way to predict the evolution of SP-onset El Niños using their onset locations.

Plain Language Summary Conventionally, the initiation, development, and decay of El Niño events were considered to be primarily controlled by atmosphere-ocean coupled processes within the tropical Pacific. Recently, studies began to suggest that more and more El Niño events were initiated by subtropical Pacific processes (simply, SP-onset El Niños). In this study, we find that this type of events tends to decay in a diverse way more than the conventional El Niños do. By analyzing a long-term simulation from a state-of-the-art climate model, we uncover the reasons why some SP-onset El Niños transition into a La Niña phase after they peak (becoming single-year events), while some others are able to linger or even re-intensify after they peak (becoming multiyear events). The longitudinal location where the event starts to develop determines if the event is capable of activiating Indo-Pacific interactions to evolve as a single-year event or tropical-subtropical Pacific interactions to evolve as a multiyear event. The findings offer the potential for use of the onset location of SP-onset El Niño to predict how the event should evolve in its decaying year.

1. Introduction

Not all El Niño–Southern Oscillation (ENSO) events are the same. Understanding the complex ENSO properties and their underlying causes has been a topic of intense research in recent years (Timmermann et al., 2018, for a review). Studies of ENSO complexity have focused more on the different spatial patterns of ENSO events and have suggested that there are at least two different types of El Niño (Capotondi et al., 2015; C. Wang, Deser, et al., 2017; L. Wang, Yu, et al., 2017; Yu et al., 2017, for reviews). These two types are often referred to as the Eastern Pacific (EP) and Central Pacific (CP) types (Kao & Yu, 2009; Yu & Kao, 2007), showing that the EP-type has its maximum sea surface temperature anomalies (SSTAs) in the tropical eastern Pacific, while the CP-type has its maximum SSTAs in the tropical central Pacific. Meanwhile, La Niña events are known to have less diversity in their spatial patterns (Chen et al., 2015; Kug & Ham, 2011).

Besides the spatial complexity, complexities have also been noted in the event-to-event evolutions of El Niño and La Niña (Kessler, 2002; Larkin & Harrison, 2002; Yu & Fang, 2018; hereafter YF18). Researchers have focused on three evolution patterns. An El Niño can be followed by a La Niña, or vice versa, to result in a cyclic ENSO evolution. Alternatively, an El Niño (La Niña) can be followed by another El Niño (La Niña) to result in a multiyear ENSO evolution. There are also events preceded or followed by a neutral phase of ENSO (i.e., neither El Niño nor La Niña), resulting in an episodic ENSO evolution. Efforts have been made to better understand the causes of these different evolution patterns and to make use of the understandings to improve ENSO predictability (An & Kim, 2017, 2018; Choi et al, 2013; DiNezio & Deser, 2014;

Dommenget et al., 2013; Kim & Yu, 2020; Lee et al., 2014; Luo et al., 2017; McGregor et al., 2012; McPhaden & Zhang, 2009; Ohba & Ueda, 2007; Okumura & Deser, 2010; Okumura et al., 2017, 2011; Park et al., 2020; B. Wang et al., 2019; Wu et al., 2019; YF18).

Conventional ENSO theories emphasized air-sea coupled processes within the tropical Pacific to explain the initiation, development, and decay of ENSO evolution, such as the delayed (Suarez & Schopf, 1988) and charged-discharged (Jin, 1997) oscillators. The tropical Pacific (TP) processes invoke wind-forced thermocline variations to initiate ENSO event by producing SSTAs in the eastern equatorial Pacific (EEP). Recent studies have increasingly emphasized that air-sea coupled processes over the subtropical Pacific can initiate ENSO event in the central equatorial Pacific (CEP) to give rise to the CP-type ENSO event (Chang et al., 2007; Di Lorenzo et al., 2015; Yu et al., 2010). The subtropical Pacific (SP) processes invoke a wind-evaporation-SST (WES) feedback (Xie & Philander, 1994) and/or trade wind charging mechanism (Anderson et al., 2013) to bring SSTAs from the northeastern subtropical Pacific to the CEP to start an ENSO event. YF18 finds that ENSO events initiated by SP processes (namely, SP-onset mechanism) can evolve in all three cyclic, multiyear, and episodic evolution patterns, while those initiated by TP processes (namely, TP-onset mechanism) mostly evolve in a cyclic evolution pattern.

The findings from YF18 indicate that the SP-onset mechanism is more important than the TP-onset mechanism for increasing the event-to-event complexity of ENSO evolution. Since ENSO predictability can be improved by recognizing which factor(s) determine the diverse evolution patterns of ENSO events, understanding the impact of the SP-onset mechanism on ENSO evolution can greatly help improve prediction. In this study, we specifically focus on the analysis of El Niño events initiated by the SP-onset mechanism (hereafter, SP-onset El Niños). We show that the onset locations where SP-onset El Niños first appear play a critical role in controlling their decay evolutions through various interbasin and basinwide interactions. As demonstrated in YF18 and Fang and Yu (2020), the SP-onset mechanism responds asymmetrically to the warm (i.e., El Niño) and cold (i.e., La Niña) phases of ENSO; thus, we solely conduct analysis on the SP-onset El Niños. The evolution diversity for the SP-onset La Niñas will be examined in a separated study.

2. Data and Methods

We analyzed four types of monthly observational datasets for the period of 1958–2019. The SST data was obtained from the Hadley Center Sea Ice and Sea Surface Temperature, version 1.1 (HadISSTv1.1; Rayner et al., 2003). The atmospheric data of zonal and meridional wind components and vertical pressure velocity were obtained from the National Centers for Environmental Prediction/National Center for Atmospheric Research Reanalysis 1 (NCEP/NCAR-R1; Kalnay et al., 1996). The sea surface height data was obtained from merging two datasets, following Kim and An (2018): the Simple Ocean Data Assimilation, version 2.2.4 (SODAv2.2.4; Carton & Giese, 2008) from 1958 to 2010, and the Global Ocean Data Assimilation System (GODAS; Behringer & Xue, 2004) from 2011 to 2019.

Due to the limited ENSO events in the observations, we also analyzed a long-term (2,200-year) simulation from the Community Earth System Model, version 1 (CESM1; Kay et al., 2015). This CESM1 simulation is a fully coupled simulation conducted at approximately 1° horizontal resolution under preindustrial greenhouse gas concentrations. We analyzed the model years 400–2200, during which the model exhibits a negligible SST trend and a minor drift in global ocean temperature. Previous studies have documented that the CESM1 realistically reproduces the observed spatiotemporal characteristics of ENSO, such as its reoccurrence frequencies, amplitude ranges, spatial structures, and temporal evolutions (e.g., DiNezio et al., 2017; Kim & Yu, 2020).

For the observational analysis, 22 El Niños were identified during the analysis period (see Table S1). Following the Climate Prediction Center, an El Niño was defined when the value of a 3-month running mean Niño3.4 index (i.e., SSTAs averaged in 5°S–5°N and 170–120°W) is at or above 0.5°C for a minimum of five consecutive overlapping seasons. For the model analysis, 352 El Niños were detected during the model years 400–2200. An El Niño was defined when the first winter (November^{0}–January^{+1}) Niño3.4 index in the CESM1 simulation is greater than its 0.5 standard deviation (0.57°C). All seasons used here were for the Northern Hemisphere. Any calendar month during the year when El Niño develops was denoted as month^{0} and that during the following year when El Niño decays was denoted as month^{+1}. Anomalies were defined

as departures from climatological values for each calendar month after removing their linear trends. Statistical analysis methods such as composite and regression analyses were applied to diagnose the anomalies. An interquartile range between the 25th and 75th percentiles was employed to describe the values of the middle 50% in the evolution pattern plots.

3. Results

3.1. Evolution Characteristics of SP-Onset El Niños in the Observations and CESM1 Simulation

We first determine if an El Niño is an SP- or TP-onset event by comparing the values of two onset indices: the SP- and TP-onset indices (see Text S1 for details). As shown in YF18, the onset of an ENSO event is most highly correlated with the SP-onset index in the preceding spring and the TP-onset index in the preceding summer (cf. Figure S1). Therefore, an El Niño was determined to be an SP-onset event if the preceding spring (March^0–May^0) SP-onset index is greater than the preceding summer (June^0–August^0) TP-onset index and is also greater than 0.5 standard deviation (to ensure the onset mechanism is in effect). The opposite case was determined to be a TP-onset event. Events that had comparable SP- and TP-onset index values with less than a 0.5 difference between them were categorized as mixed-onset El Niños. As a result, we identified 6 SP-onset and 7 TP-onset El Niños in the observations and 139 SP-onset and 155 TP-onset El Niños in the CESM1 simulation (see Tables S1 and S2). The sample size of the simulated SP-onset El Niños is about 20 times larger than the observation sample size. Furthermore, 47% of El Niños in the simulation are SP-onset El Niños, which is very close to the percentage of SP-onset El Niños in the observations (46%).

We performed a composite analysis with the SP-onset events to examine their evolution characteristics. In the observations (Figure 1a), the warm SSTAs of SP-onset El Niño first emerge in the CEP during spring (lying to the west of the dateline; cf. black vertical line in Figure 1a). The initial warm anomalies then develop and extend eastward during the following summer and fall, covering the equatorial Pacific. The event peaks in winter with its maximum warming located around 165°W. These warm anomalies thereafter do not decay and transition into a La Niña in the following year. Instead, they linger and slowly decay in the CEP during the subsequent seasons, exhibiting multiyear evolution. The composite evolution of the Niño3.4 index (black curve in Figure 1b) clearly shows this multiyear evolution. The six individual SP-onset El Niños (gray curves in Figure 1b) evolve similarly during their development stages; however, they dramatically diverge from each other during their decay stages. As shown in Table S1, half of the observed SP-onset El Niños exhibit a cyclic evolution (i.e., second winter Niño3.4 index < 0); the other half exhibit a multiyear evolution (i.e., second winter Niño3.4 index > 0). The above results collectively indicate that SP-onset El Niños have a large complexity and therefore uncertainties, in their decay evolutions. This is the crucial part of El Niño evolutions that needs to be better understood to improve ENSO prediction.

We repeated the same composite analysis but with a much larger sample size in the CESM1 simulation to examine the robustness of the observational results. Despite some discrepancies such as the presence of warm anomalies originating from the far-EEP during the developing year, the simulation (Figure 1c) generally reproduces the key evolution features of the observed SP-onset El Niño: the warm SSTAs first emerging in the CEP, extending eastward as the event develops until its peak, then lingering in the following year after the peak. The composite evolution of the Niño3.4 index for the simulated SP-onset El Niños (black curve in Figure 1d) exhibits a multiyear evolution, resembling the observed one. The interquartile ranges (gray shading in Figure 1d) also reveal that the simulated events evolve similarly during their development stages but very differently after they peak. Indeed, 51% of the simulated SP-onset El Niños have cyclic evolution and 49% have multiyear evolution (see Table S2); these percentages are nearly the same as the observations. This proves that the CESM1 simulation is appropriate for the study of SP-onset El Niños.

We then checked whether the large uncertainty in the decay evolution is unique to SP-onset El Niños or if it can also be found in TP-onset El Niños. Results from the composite analysis (Figure S2) illustrate that the TP-onset El Niños have a smaller event-to-event difference (thus, less uncertainty) in their decay evolutions. Most TP-onset El Niños in the observations (86%) and CESM1 simulation (70%) undergo phase transition to La Niñas after they peak, leading to cyclic evolution (cf. Tables S1 and S2). These results support the findings from YF18 and Fang and Yu (2020) that most TP-onset ENSO events have cyclic evolution and that the SP-onset mechanism is a key source for ENSO evolution complexity.

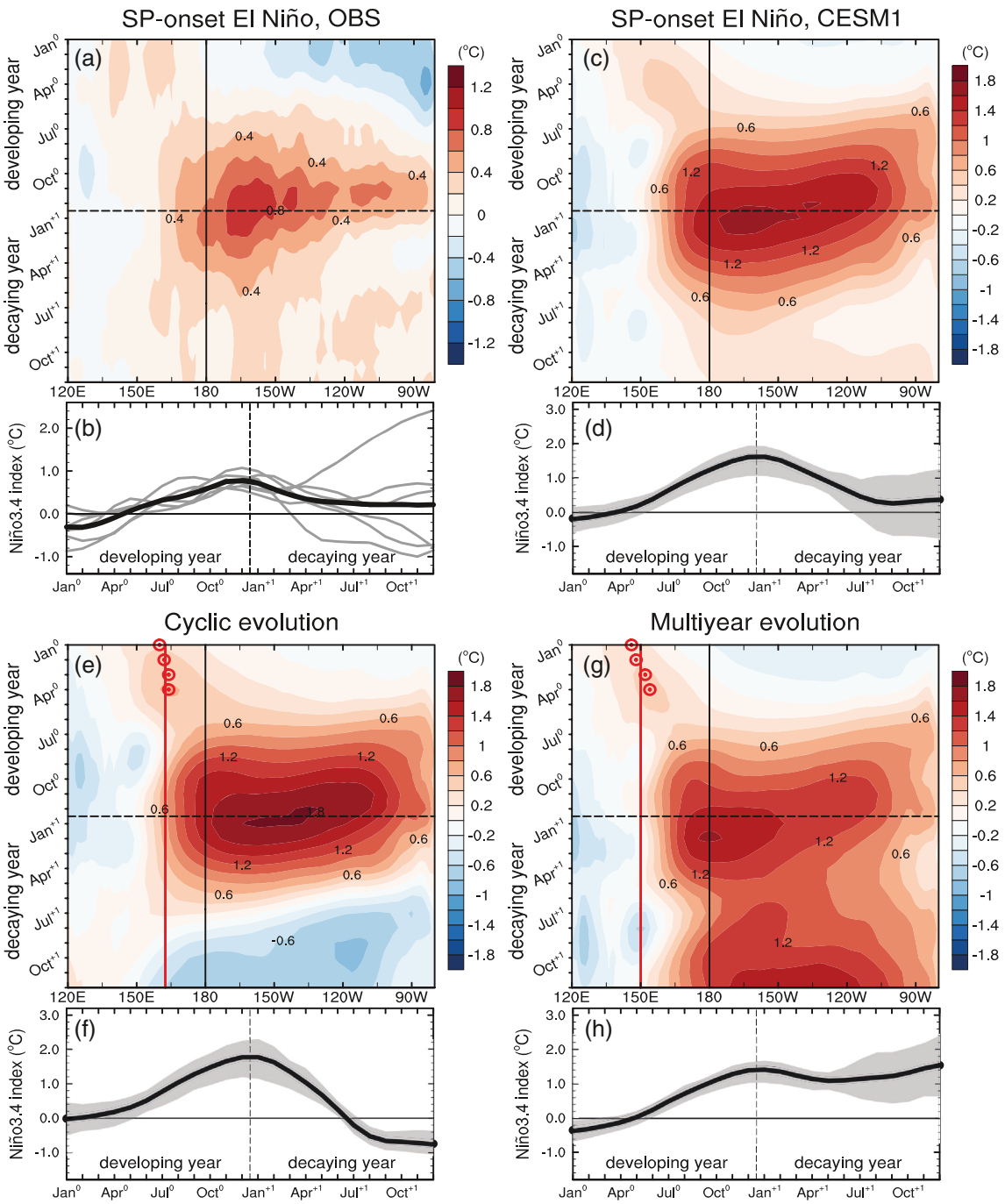

Figure 1. Composite structures and evolutions of SP-onset El Niños. (a and b) Longitude-time plot of equatorial (i.e., 5°S–5°N) SSTAs during the developing and decaying years from January^{0} to December^{+1} for the observations is presented in the upper panel. Temporal evolution of the Niño3.4 index during the developing and decaying years in the observations is presented in the lower panel. The gray curves in (b) indicates individual event evolutions. (c and d) are the same as (a and b) except for the CESM1 simulation and the gray shading in (d) indicates interquartile ranges between the 25th and 75th percentiles. (e and f) and (g and h) are the same as (c and d), respectively, except for the cyclic and multiyear evolution events. In (e) and (g), the red circled dots mark the maximum warm SSTAs from January^{0} to April^{0} and the red vertical lines denote their averaged longitudinal positions. SSTAs, sea surface temperature anomalies.

3.2. Linking Onset Locations to the Evolution Patterns of SP-Onset El Niños

It is important to know if there is any key factor determining whether an SP-onset El Niño should decay in a cyclic or multiyear evolution. For this purpose, we contrasted the composite analyses between cyclic and multiyear evolution groups of SP-onset events in the CESM1 simulation. As seen in Table S2, there are 71

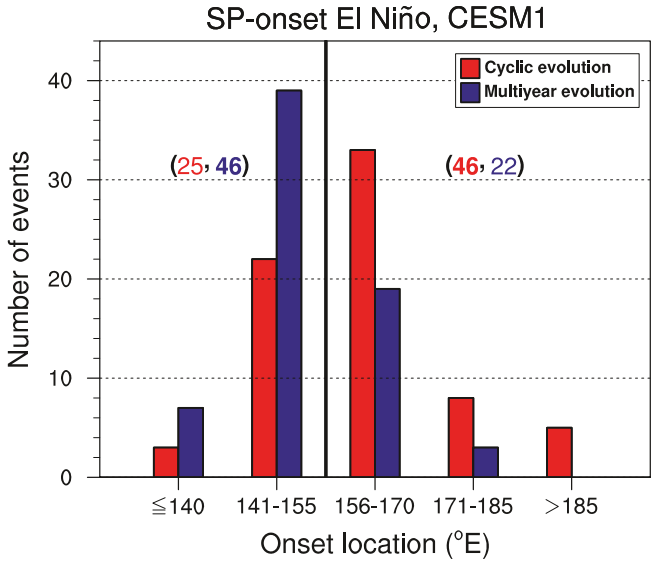

Figure 2. The number of SP-onset El Niños in the CESM1 simulation categorized as cyclic (red bar-chart) and multiyear (blue bar-chart) evolutions as the onset location shifts in 15-degree intervals from 140°E to 185°E in the longitudinal direction. The onset location is quantitatively measured from the mean longitude of the maximum warm SSTAs averaged over the equator (i.e., 5°S–5°N) during the developing spring from March^0 to May^0. The total number of cyclic and multiyear evolutions occurring when the onset is located east or west of 155°E are shown as red and blue text (with larger numbers in bold), respectively.

cyclic and 68 multiyear SP-onset El Niños in the simulation. Figure 1e and 1g indicate that, although both El Niño evolution patterns have initial warm anomalies in the CEP during spring, the exact onset locations are different. The cyclic evolution group (Figure 1e) has its onset location around 165°E (close to the dateline), while the multiyear evolution group (Figure 1g) has its onset location around 150°E (further away from the dateline). There are about 15 degrees of longitudinal difference between these two groups. After the El Niños develop, the cyclic evolution group peaks near 150°W and has maximum SSTAs over the EEP. In contrast, the multiyear evolution group peaks at the dateline and has maximum SSTAs over the CEP (note that the longitudinal difference increases to around 30° between their peak locations). Shortly thereafter, the cyclic evolution group decays rapidly and transitions into a La Niña condition, while the multiyear evolution group lingers and subsequently re-intensifies into another El Niño condition. The composite evolutions of the Niño3.4 index and their interquartile ranges displayed in Figure 1f and 1h further reveal the abovementioned cyclic and multiyear evolutions, with the former (latter) having negative (positive) index values during their decay evolutions. The relatively larger interquartile ranges during the decay evolution of multiyear events are due to the fact that some multiyear El Niños re-intensify into larger amplitudes in the second year while some others linger in the warm phase with a slow decay. The physical processes responsible for the re-intensified multiyear El Niños have been identified in Kim and Yu (2020).

The above analyses suggest that the onset location of SP-onset El Niño may play a role in controlling its decay evolution. To examine this possibility, we counted the numbers of cyclic and multiyear evolution events as their onset locations shift from 140°E to 185°E. Here the onset location for each event is calculated as the mean longitude of the maximum warm SSTAs during the developing spring from March^0 to May^0. The results displayed in Figure 2 show a strong tendency for cyclic (multiyear) evolution to occur more frequently than multiyear (cyclic) evolution as the onset location is shifted eastward (westward). If we take 155°E as a dividing longitude, 68% of SP-onset El Niños whose onsets are located to the east of this longitude have cyclic evolution (i.e., 46 out of 68 events). Conversely, 65% of SP-onset El Niños whose onsets are located to the west of this longitude have multiyear evolution (i.e., 46 out of 71 events). These contrasting tendencies indicate that SP-onset El Niños have selective dominance toward either cyclic or multiyear evolution according to their onset locations (e.g., east of 155°E vs. west of 155°E). The above result is not sensitive to a little change in the criterion, such as moving the criterion longitude from 150°E to 160°E (Figure S3).

3.3. Physical Mechanisms Behind the Linkage

To understand the physical processes of how the SP-onset El Niño's onset location controls its decay evolution, a conditional composite analysis was carried out using two groups of events in the CESM1 simulation. The first group (Group-A) consists of SP-onset El Niños whose onset locations reside east of 155°E and have cyclic evolution, indicating that they transition to a La Niña condition in the following year. The second group (Group-B) is defined as SP-onset El Niños that have onset locations west of 155°E and multiyear evolution. The El Niños in this group linger or re-intensify into another El Niño condition in the following year. As shown in Figure 2, each group equally has 46 events.

Using the two groups defined above, we first explain how the eastward-shifted onset enables SP-onset El Niños to undergo cyclic evolution more often. For the Group-A events, the initial warm SSTAs during spring (lower panel of Figure 3a) are located over the CEP, with their maximum intensity around 165°E. Since the onset location is on the eastern edge of the western Pacific warm pool (green contour in the lower panel of Figure 3a), the warm anomalies can easily increase local SSTs from below the convective threshold

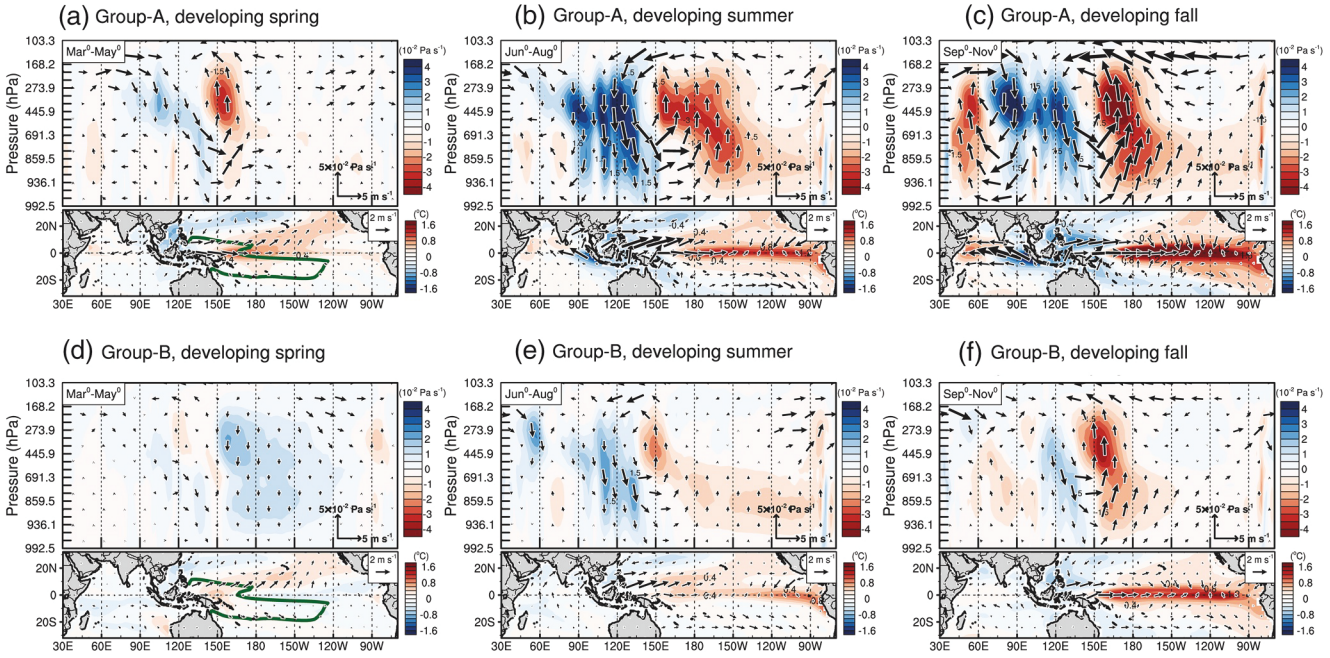

Figure 3. Composite structures over the Indian and Pacific Oceans for the Group-A events of SP-onset El Niños in the CESM1 simulation during the developing (a) spring, (b) summer, and (c) fall. Equatorially (i.e., 5°S–5°N) averaged anomalous omega field (shadings; in 10^{-2} Pa s^{-1}) and zonal overturning cell (vectors; computed by the anomalous omega field and zonal wind component) are presented in the upper panel. The omega field is used after multiplying a scale factor of 100. Anomalous SST (shadings; in °C) and surface wind (vectors; in m s^{-1}) are presented in the lower panel. (d–f) Same as (a–c), respectively, except for the Group-B events. The green contours in (a) and (d) denote climatological 28°C isotherm line which depicts an area for the western Pacific warm pool during spring.

temperature to above it (~28°C; cf. Sud et al., 1999; Zhang, 1993). As a result, the small initial SSTAs excite deep convection, producing a large heating anomaly in the atmosphere (e.g., Fang & Yu, 2020). The anomalous heating, in turn, induces a zonal overturning cell anomaly over the tropical western Pacific (upper panel of Figure 3a). Strong westerly anomalies are simultaneously generated near the surface, with their maximum intensity located to the west of the onset SSTAs (lower panel of Figure 3a). In the following summer, the strong westerly anomalies push the underlying warm SSTAs to the east by exciting downwelling Kelvin waves that lead to EEP warming (lower panel of Figure 3b). The warming in the EEP subsequently triggers the Bjerknes feedback (Bjerknes, 1969) which involves a positive feedback process between equatorial trade winds and the underlying zonal SST gradients that further amplifies the initial El Niño warming. This Bjerknes feedback also involves a shift in the atmospheric convection toward the east, causing a change in the Walker circulation along with an ascending (descending) anomaly over the CEP-to-EEP (Maritime continent) (upper panel of Figure 3b). The descending anomaly over the Maritime continent induces strong divergent surface winds with westerly (easterly) anomalies over the tropical western Pacific (eastern Indian Ocean) (lower panel of Figure 3b). As the season changes from summer to fall (Figure 3c), the Bjerknes feedback in the Pacific strengthens the El Niño amplitude. Meanwhile, the easterly anomalies over the eastern Indian Ocean give rise to a positive phase of the Indian Ocean Dipole (IOD; Saji et al., 1999).

Compared to Group-A, composite structures of the Group-B events during spring (Figure 3d) show more westward-shifted onset location with initial warm SSTAs occurring inside the warm pool (lower panel of Figure 3d). Since the deep convection is already most active within the warm pool, the small initial SSTAs induce small increases in the deep convection, producing a small heating anomaly in the atmosphere. This leads to a much weaker zonal overturning cell anomaly over the tropical western Pacific (Figure 3a vs. Figure 3d). Thus, westerly anomalies are also weakly generated near the surface to the west of the onset SSTAs (lower panel of Figure 3d). In the following summer (Figure 3e), the weak westerly anomalies cause a small EEP warming through dimly excited downwelling Kelvin waves. It then triggers a weak Bjerknes feedback in the Pacific with no noticeable Walker circulation change (upper panel of Figure 3e; cf. the zonal overturning cell anomaly over the tropical western Pacific is likely due to the underlying SSTAs that exceed

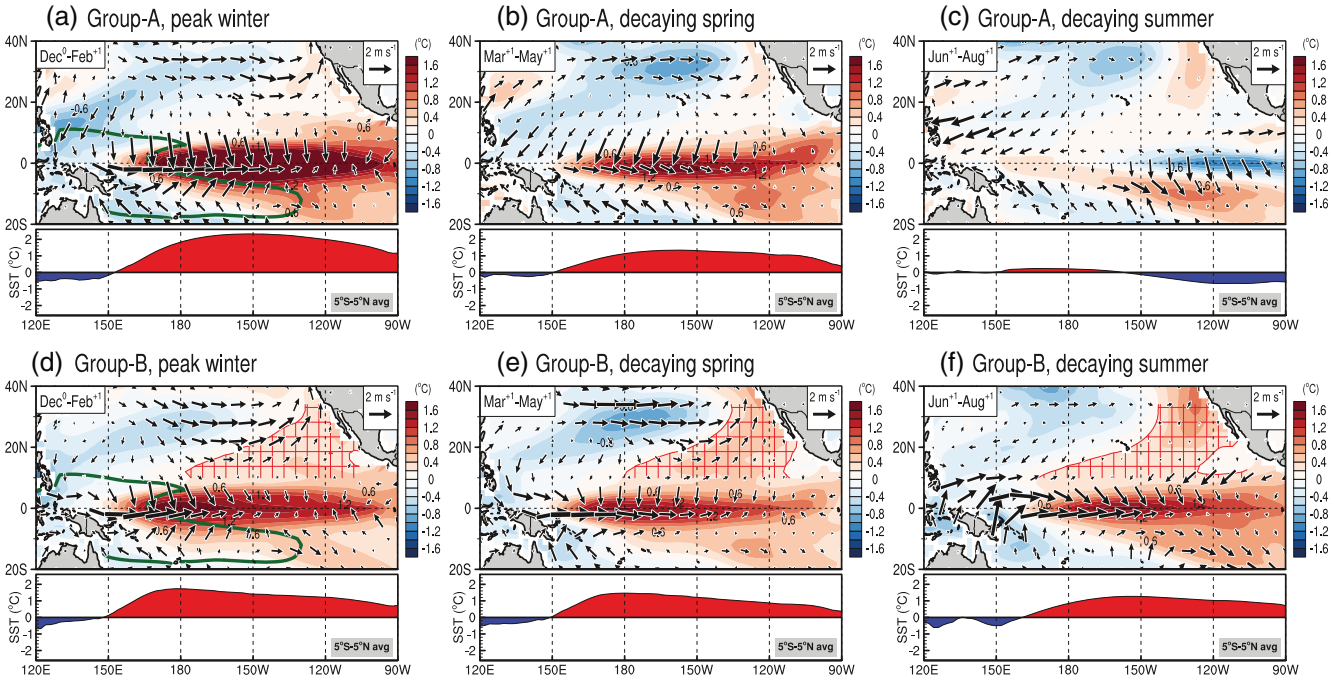

Figure 4. Composite structures over the Pacific Ocean for the Group-A events of SP-onset El Niños in the CESM1 simulation during the (a) peak winter and the (b) decaying spring and (c) summer. Anomalous SST (shadings; in °C) and surface wind (vectors; in m s^{-1}) are presented in upper panel. Equatorially (i.e., 5°S–5°N) averaged zonal structures of SST anomaly are presented in the lower panel. (d–f) Same as (a–c), respectively, except for the Group-B events. the green contours in (a) and (d) denote climatological 28°C isotherm line which depicts an area for the western Pacific warm pool during winter. The red cross-hatched sectors in (d–f) denote subtropical areas with temperature greater than 0.2°C signifying the area in which a positive PMM occurs.

the convective threshold). As the season moves toward fall (Figure 3f), the weak Bjerknes feedback leads to an El Niño that has a relatively weak amplitude. Meanwhile, there are no IOD-related SST and surface wind anomalies over the Indian Ocean. This is because, unlike the Group-A events, the change in the Walker circulation for the Group-B events is too weak to activate interbasin interactions between the Pacific and Indian Oceans (Figure 3c vs. Figure 3f).

Previous studies (Cai et al., 2019; Izumo et al., 2010; Kug & Kang, 2006) have shown that a positive IOD can hasten the termination of El Niño and transition its phase to La Niña by reversing surface wind anomalies over the tropical western Pacific from westerly to easterly during winter and following spring, which excite upwelling Kelvin waves that subsequently trigger La Niña conditions. This transition effect of the IOD can be confirmed by a lagged regression with an IOD index (see Text S2 and Figure S4). Consistent with the abovementioned IOD effect, the Group-A events, which have a strong positive IOD in the developing year due to their eastward onset locations, decay rapidly and transition to La Niña, thereby having cyclic evolution (Figure S5a). In contrast, the Group-B events do not have an IOD event due to their westward onset locations; thus, the IOD's transition effect on this group of events does not occur and, instead, they have multiyear evolution (Figure S5b). This is one reason why the Group-B events do not transition to La Niña after they peak.

Still, a physical mechanism is required to explain why the Group-B events maintain El Niño conditions for another year, resulting in multiyear evolution. During the peak-to-decaying seasons for Group-B (Figures 4d–4f), we notice a band of warm SSTAs extending from the subtropical Pacific to the CEP (cf. red cross-hatched sectors in Figures 4d–4f) closely resembling a positive phase of the Pacific Meridional Mode (PMM; Chiang & Vimont, 2004). The PMM, once it begins, is able to maintain itself for several seasons and extends equatorward through the WES feedback (which involves a positive feedback process between subtropical trade wind anomalies and the underlying warm SSTAs by reducing the ocean surface's evaporation rate), subsequently spreading warm anomalies into the equatorial Pacific basin (cf. Amaya, 2019; Yu & Kim, 2011; Yu et al., 2010). This PMM-related warm SSTA band is however very weak during the

peak-to-decaying seasons for Group-A (Figures 4a–4c). Thus, as can be inferred from Figure 4, we suggest that Group-B events more easily excite the PMM (as compared to Group-A events) and lead the El Niño to multiyear evolution via activation of tropical-subtropical Pacific interactions. Since El Niño warming of Group-B events during the peak winter is located near the warm pool where background SSTs are already very close to the convective threshold (Figure 4d), it easily excites deep convection over the CEP and triggers an atmospheric Rossby wave train. This Rossby wave train induces a lower-tropospheric anomalous cyclone over the northeastern subtropical Pacific that activates the WES feedback there, thereby initiating and developing a positive PMM (cf. Fang & Yu, 2020; Stuecker, 2018). The positive PMM, in turn, leads to the multiyear evolution of Group-B events by spreading warm SSTAs into the equatorial Pacific in the subsequent seasons. These basinwide interactions between the tropical and subtropical Pacific are more unlikely to occur for Group-A events as their El Niño warming is located further away from the warm pool (Figure 4a); therefore, Group A events struggle to excite deep convection over the CEP. This explains why Group-B events are more capable of maintaining El Niño conditions than Group-A events and result in multiyear evolution. A lagged regression analysis using a PMM index also supports our suggestion (see Text S2 and Figure S6).

In addition to the Indo-Pacific and tropical-subtropical Pacific interactions, it may also be possible that anomalous SST warming over the north tropical Atlantic (NTA), which can be driven by an El Niño-associated teleconnection pattern after the El Niño's peak (e.g., Enfield & Mayer, 1997; Saravanan & Chang, 2000), influences the decay evolution of SP-onset El Niño as it subsequently induces easterly anomalies over the tropical western Pacific (Ham et al., 2013; C. Wang, Deser, et al., 2017; L. Wang, Yu, et al., 2017). Our additional analyses, however, did not show any strong evidence to support the above possibility (see Text S3 and Figure S7 for details). This implies that the anomalous NTA SST warming in the decaying spring, at least in this study, does not play a role in controlling the decay evolution of SP-onset El Niño.

Despite the limited number of observed SP-onset El Niños, we found two observational events that are most consistent with the findings of this study: the 1994–1995 and 1968–1969 events (Figure S8). The 1994–1995 event was characterized by an eastward onset location (~170°E) and a cyclic evolution. This event was accompanied by a very strong positive IOD (>2 s.d) during its developing summer-to-fall while the PMM was very weak (<±1 s.d.) during its peak winter-to-decaying spring—a reflection of strong Indo-Pacific interactions. On the other hand, the 1968–1969 event was characterized by a westward onset location (~140°E) and a multiyear evolution. This event had a strong positive PMM (>1 s.d) during its peak winter-to-decaying spring but a weak negative IOD during its developing summer-to-fall (<0 s.d.)—a reflection of strong tropical-subtropical Pacific interactions.

4. Concluding Remarks

This study used observations and a long-term CESM1 simulation to understand why SP-onset El Niños have diverse evolution patterns after their peaks (about half of the events exhibiting cyclic evolution and the other half exhibiting multiyear evolution); contrastingly, most TP-onset El Niños transitioned to La Niña after their peaks, exhibiting cyclic evolution. These observed contrasting evolution patterns of the SP- and TP-onset El Niños were realistically reproduced in the CESM1 simulation with a much larger number of simulated events.

It is concluded that the evolution patterns are very sensitive to the exact onset locations of SP-onset El Niños. The eastward-shifted onset events (Group-A, this study) are more capable of activating Indo-Pacific interactions, while the westward-shifted onset events (Group-B, this study) are more capable of activating tropical-subtropical Pacific interactions. The Indo-Pacific interactions reverse the El Niños to La Niña conditions, resulting in cyclic evolution. The tropical-subtropical Pacific interactions maintain El Niño conditions, producing multiyear evolution. The descending/ascending locations of the Walker circulation enable the eastward-shifted events to more strongly activate the Indo-Pacific interactions during El Niño's developing phase, while the enhanced background SSTs near the western Pacific warm pool enable the westward-shifted events to more strongly activate the tropical-subtropical Pacific interactions during El Niño's peak phase. The findings of this study offer new insight into understanding the diverse evolutions of SP-onset El Niños and uncover the potential for the onset locations of SP-onset El Niños to predict their evolutions in the following year.

Since there is a relatively stronger onset intensity in Group-A than Group-B (cf. lower panels of Figure 3a and 3d), the possibility that diverse evolutions of SP-onset El Niños may also be related to their different onset intensities should be addressed as well. To examine this, we computed regression coefficients of surface wind anomalies with respect to SSTAs on the equator at 165°E and 150°E (representing the onset locations of Group-A and Group-B, respectively). The regression coefficients allow us to assess how the surface wind anomalies are related to a unit change of SST forcing (thus, m s^{-1}/°C) at its two different onset locations (at 165°E vs. at 150°E). As a result, the regression maps (Figure S9a and S9b) showed that there is a noticeable difference between the two onset locations. Stronger, more eastward-shifted westerly anomalies occur when the onset is at 165°E (i.e., on the eastern edge of the warm pool) but weaker, more westward-shifted westerly anomalies occur when the onset is at 150°E (i.e., inside the warm pool). The equatorially (i.e., 5°S–5°N) averaged zonal structures for the regression coefficients (Figure S9c) further support this by revealing the longitudinal shift of wind anomalies between the two onset locations (note that the difference in the tropical western Pacific wind anomalies is a key element producing the diverse evolutions of SP-onset El Niño; cf. Section 3.3). From the results above, it is reasonable to infer that any possible controlling effect on the evolutions of SP-onset El Niños caused by different onset intensities would likely not diminish the controlling effect caused by different onset locations, as found in this study.

The question of what process(es) determine the onset location of SP-onset El Niño remained unanswered in the present study. In this regard, there are at least two possibilities. The first possibility is that it may just happen by chance under the stochastically driven random scenarios. The second possibility is that subtle differences in the subtropical trade wind anomalies that trigger the SP-onset mechanism may cause the PMM patterns to vary and initiate El Niños at different locations. The latter possibility has to be carefully examined in a future study.

Finally, we did not include the mixed-onset El Niños in the analysis because the purpose of the present study was to understand the evolutions of "pure" SP-onset El Niños. Hence, understanding how the TP- and SP-onset mechanisms interfere with each other and shape the evolutions of mixed-onset El Niños is another interesting research topic that deserves to be explored in future studies.

Data Availability Statement

The 2,200-year CESM1 simulation was conducted by the CESM project team and are available via the Earth System Grid (https://www.earthsystemgrid.org/). The HadISSTv1.1 data were downloaded from the Met Office Hadley Center (https://www.metoffice.gov.uk/hadobs/). The NCEP/NCAR-R1 data were obtained from their website (https://www.esrl.noaa.gov/psd/data/gridded/data.ncep.reanalysis.html). The SODAv2.2.4 data were obtained from their website (https://coastwatch.pfeg.noaa.gov/erddap/griddap/hawaii_d90f_20ee_c4cb.html) and the GODAS data were downloaded from their website (https://www.esrl.noaa.gov/psd/data/gridded/data.godas.html).

Acknowledgments
The authors thank the two anonymous reviewers whose helpful suggestions and comments improved this study greatly. The authors are also very grateful to all data providers. This research was supported by NSF Climate and Large-Scale Dynamics Program under grant AGS-1833075.

References

Amaya, D. J. (2019). The Pacific meridional mode and ENSO: A review. *Current Climate Change Reports*, *5*(4), 296–307.

An, S. I., & Kim, J. W. (2017). Role of nonlinear ocean dynamic response to wind on the asymmetrical transition of El Niño and La Niña. *Geophysical Research Letters*, *44*(1), 393–400. https://doi.org/10.1002/2016GL071971

An, S. I., & Kim, J. W. (2018). ENSO transition asymmetry: Internal and external causes and intermodel diversity. *Geophysical Research Letters*, *45*(10), 5095–5104. https://doi.org/10.1029/2018GL078476

Anderson, B. T., Perez, R. C., & Karspeck, A. (2013). Triggering of El Niño onset through trade wind–induced charging of the equatorial Pacific. *Geophysical Research Letters*, *40*(6), 1212–1216. https://doi.org/10.1002/grl.50200

Behringer, D. W., & Xue, Y. (2004). *Evaluation of the global ocean data assimilation system at NCEP: The Pacific Ocean*. Proceedings of Eighth Symposium on Integrated Observing and Assimilation Systems for Atmosphere, Oceans, and Land Surface, AMS 84th Annual Meeting, Washington State Convention and Trade Center, Seattle, WA.

Bjerknes, J. (1969). Atmospheric teleconnections from the equatorial Pacific. *Monthly Weather Review*, *97*(3), 163–172.

Cai, W., Wu, L., Lengaigne, M., Li, T., McGregor, S., Kug, J. S., et al. (2019). Pantropical climate interactions. *Science*, *363*(6430), eaav4236.

Capotondi, A., Wittenberg, A. T., Newman, M., Di Lorenzo, E., Yu, J. Y., Braconnot, P., et al. (2015). Understanding ENSO diversity. *Bulletin of the American Meteorological Society*, *96*(6), 921–938.

Carton, J. A., & Giese, B. S. (2008). A reanalysis of ocean climate using Simple Ocean Data Assimilation (SODA). *Monthly Weather Review*, *136*(8), 2999–3017.

Chang, P., Zhang, L., Saravanan, R., Vimont, D. J., Chiang, J. C., Ji, L., et al. (2007). Pacific meridional mode and El Niño—Southern oscillation. *Geophysical Research Letters*, *34*(16). https://doi.org/10.1029/2007GL030302

Chen, D., Lian, T., Fu, C., Cane, M. A., Tang, Y., Murtugudde, R., et al. (2015). Strong influence of westerly wind bursts on El Niño diversity. *Nature Geoscience*, *8*(5), 339–345.
Chiang, J. C., & Vimont, D. J. (2004). Analogous Pacific and Atlantic meridional modes of tropical atmosphere–ocean variability. *Journal of Climate*, *17*(21), 4143–4158.
Choi, K. Y., Vecchi, G. A., & Wittenberg, A. T. (2013). ENSO transition, duration, and amplitude asymmetries: Role of the nonlinear wind stress coupling in a conceptual model. *Journal of Climate*, *26*(23), 9462–9476.
Di Lorenzo, E., Liguori, G., Schneider, N., Furtado, J. C., Anderson, B. T., & Alexander, M. A. (2015). ENSO and meridional modes: A null hypothesis for Pacific climate variability. *Geophysical Research Letters*, *42*(21), 9440–9448. https://doi.org/10.1002/2015GL066281
DiNezio, P. N., & Deser, C. (2014). Nonlinear controls on the persistence of La Niña. *Journal of Climate*, *27*(19), 7335–7355.
DiNezio, P. N., Deser, C., Okumura, Y., & Karspeck, A. (2017). Predictability of 2-year La Niña events in a coupled general circulation model. *Climate Dynamics*, *49*(11–12), 4237–4261.
Dommenget, D., Bayr, T., & Frauen, C. (2013). Analysis of the non-linearity in the pattern and time evolution of El Niño southern oscillation. *Climate Dynamics*, *40*(11–12), 2825–2847.
Enfield, D. B., & Mayer, D. A. (1997). Tropical Atlantic sea surface temperature variability and its relation to El Niño-Southern Oscillation. *Journal of Geophysical Research*, *102*(C1), 929–945.
Fang, S. W., & Yu, J. Y. (2020). A control of ENSO transition complexity by tropical Pacific mean SSTs through tropical-subtropical interaction. *Geophysical Research Letters*, *47*, e2020GL087933. (12). https://doi.org/10.1029/2020GL087933
Ham, Y. G., Kug, J. S., Park, J. Y., & Jin, F. F. (2013). Sea surface temperature in the north tropical Atlantic as a trigger for El Niño/Southern Oscillation events. *Nature Geoscience*, *6*(2), 112–116.
Izumo, T., Vialard, J., Lengaigne, M., de Boyer Montegut, C., Behera, S. K., Luo, J. J., et al. (2010). Influence of the state of the Indian Ocean Dipole on the following year's El Niño. *Nature Geoscience*, *3*(3), 168.
Jin, F. F. (1997). An equatorial ocean recharge paradigm for ENSO. Part I: Conceptual model. *Journal of the Atmospheric Sciences*, *54*(7), 811–829.
Kalnay, E., Kanamitsu, M., Kistler, R., Collins, W., Deaven, D., Gandin, L., et al. (1996). The NCEP/NCAR 40-year reanalysis project. *Bulletin of the American Meteorological Society*, *77*(3), 437–472.
Kao, H. Y., & Yu, J. Y. (2009). Contrasting eastern-Pacific and central-Pacific types of ENSO. *Journal of Climate*, *22*(3), 615–632.
Kay, J. E., Deser, C., Phillips, A., Mai, A., Hannay, C., Strand, G., et al. (2015). The Community Earth System Model (CESM) large ensemble project: A community resource for studying climate change in the presence of internal climate variability. *Bulletin of the American Meteorological Society*, *96*(8), 1333–1349.
Kessler, W. S. (2002). Is ENSO a cycle or a series of events? *Geophysical Research Letters*, *29*(23), 40–44. https://doi.org/10.1029/2002GL015924
Kim, J. W., & An, S. I. (2018). Origin of early-spring central Pacific warming as the 1982–1983 El Niño precursor. *International Journal of Climatology*, *38*(6), 2899–2906.
Kim, J. W., & Yu, J. Y. (2020). Understanding reintensified multiyear El Niño events. *Geophysical Research Letters*, *47*(12), e2020GL087644. https://doi.org/10.1029/2020GL087644
Kug, J. S., & Ham, Y. G. (2011). Are there two types of La Niña? *Geophysical Research Letters*, *38*(16). https://doi.org/10.1029/2011GL048237
Kug, J. S., & Kang, I. S. (2006). Interactive feedback between ENSO and the Indian Ocean. *Journal of Climate*, *19*(9), 1784–1801.
Larkin, N. K., & Harrison, D. E. (2002). ENSO warm (El Niño) and cold (La Niña) event life cycles: Ocean surface anomaly patterns, their symmetries, asymmetries, and implications. *Journal of Climate*, *15*(10), 1118–1140.
Lee, S. K., DiNezio, P. N., Chung, E. S., Yeh, S. W., Wittenberg, A. T., & Wang, C. (2014). Spring persistence, transition, and resurgence of El Niño. *Geophysical Research Letters*, *41*(23), 8578–8585. https://doi.org/10.1002/2014GL062484
Luo, J. J., Liu, G., Hendon, H., Alves, O., & Yamagata, T. (2017). Inter-basin sources for two-year predictability of the multiyear La Niña event in 2010–2012. *Scientific Reports*, *7*, 2276.
McGregor, S., Timmermann, A., Schneider, N., Stuecker, M. F., & England, M. H. (2012). The effect of the South Pacific convergence zone on the termination of El Niño events and the meridional asymmetry of ENSO. *Journal of Climate*, *25*(16), 5566–5586.
McPhaden, M. J., & Zhang, X. (2009). Asymmetry in zonal phase propagation of ENSO sea surface temperature anomalies. *Geophysical Research Letters*, *36*(13). https://doi.org/10.1029/2009GL038774
Ohba, M., & Ueda, H. (2007). An impact of SST anomalies in the Indian Ocean in acceleration of the El Niño to La Niña transition. *Journal of the Meteorological Society of Japan. Ser. II*, *85*(3), 335–348.
Okumura, Y. M., & Deser, C. (2010). Asymmetry in the duration of El Niño and La Niña. *Journal of Climate*, *23*(21), 5826–5843.
Okumura, Y. M., DiNezio, P., & Deser, C. (2017). Evolving impacts of multiyear La Niña events on atmospheric circulation and US drought. *Geophysical Research Letters*, *44*(22), 11614. https://doi.org/10.1002/2017GL075034
Okumura, Y. M., Ohba, M., Deser, C., & Ueda, H. (2011). A proposed mechanism for the asymmetric duration of El Niño and La Niña. *Journal of Climate*, *24*(15), 3822–3829.
Park, J. H., An, S. I., Kug, J. S., Yang, Y. M., Li, T., & Jo, H. S. (2020). Mid-latitude leading double-dip La Niña. *International Journal of Climatology*, *41*, E1353–E1370.
Rayner, N. A. A., Parker, D. E., Horton, E. B., Folland, C. K., Alexander, L. V., Rowell, D. P., et al. (2003). Global analyses of sea surface temperature, sea ice, and night marine air temperature since the late nineteenth century. *Journal of Geophysical Research: Atmospheres*, *108*(D14). https://doi.org/10.1029/2002JD002670
Saji, N. H., Goswami, B. N., Vinayachandran, P. N., & Yamagata, T. (1999). A dipole mode in the tropical Indian Ocean. *Nature*, *401*(6751), 360.
Saravanan, R., & Chang, P. (2000). Interaction between tropical Atlantic variability and El Niño–Southern oscillation. *Journal of Climate*, *13*(13), 2177–2194.
Stuecker, M. F. (2018). Revisiting the Pacific meridional mode. *Scientific Reports*, *8*(1), 1–9.
Suarez, M. J., & Schopf, P. S. (1988). A delayed action oscillator for ENSO. *Journal of the Atmospheric Sciences*, *45*(21), 3283–3287.
Sud, Y. C., Walker, G. K., & Lau, K. M. (1999). Mechanisms regulating sea-surface temperatures and deep convection in the tropics. *Geophysical Research Letters*, *26*(8), 1019–1022.
Timmermann, A., An, S. I., Kug, J. S., Jin, F. F., Cai, W., Capotondi, A., et al. (2018). El Niño–Southern Oscillation complexity. *Nature*, *559*(7715), 535–545.
Wang, B., Luo, X., Yang, Y. M., Sun, W., Cane, M. A., Cai, W., et al. (2019). Historical change of El Niño properties sheds light on future changes of extreme El Niño. *Proceedings of the National Academy of Sciences of the United States of America*, *116*(45), 22512–22517.
Wang, C., Deser, C., Yu, J. Y., DiNezio, P., & Clement, A. (2017). El Niño and southern oscillation (ENSO): A review. In P. W. Glynn, D. P. Manzello, I. C. Enochs (Eds.), *Coral reefs of the eastern tropical Pacific* (pp. 85–106). Dordrecht, The Netherlands: Springer.

Wang, L., Yu, J. Y., & Paek, H. (2017). Enhanced biennial variability in the Pacific due to Atlantic capacitor effect. *Nature Communications*, *8*(1), 1–7.

Wu, X., Okumura, Y. M., & DiNezio, P. N. (2019). What controls the duration of El Niño and La Niña Events? *Journal of Climate*, *32*(18), 5941–5965.

Xie, S. P., & Philander, S. G. H. (1994). A coupled ocean-atmosphere model of relevance to the ITCZ in the eastern Pacific. *Tellus A*, *46*(4), 340–350.

Yu, J. Y., & Fang, S. W. (2018). The distinct contributions of the seasonal footprinting and charged-discharged mechanisms to ENSO complexity. *Geophysical Research Letters*, *45*(13), 6611–6618. https://doi.org/10.1029/2018GL077664

Yu, J. Y., & Kao, H. Y. (2007). Decadal changes of ENSO persistence barrier in SST and ocean heat content indices: 1958–2001. *Journal of Geophysical Research*, *112*(D13). https://doi.org/10.1029/2006JD007654

Yu, J. Y., Kao, H. Y., & Lee, T. (2010). Subtropics-related interannual sea surface temperature variability in the central equatorial Pacific. *Journal of Climate*, *23*(11), 2869–2884.

Yu, J. Y., & Kim, S. T. (2011). Relationships between extratropical sea level pressure variations and the central Pacific and eastern Pacific types of ENSO. *Journal of Climate*, *24*(3), 708–720.

Yu, J. Y., Wang, X., Yang, S., Paek, H., & Chen, M. (2017). *The changing El Niño–Southern Oscillation and associated climate extremes* (pp. 1–38). Hoboken, NJ: John Wiley & Sons, Inc..

Zhang, C. (1993). Large-scale variability of atmospheric deep convection in relation to sea surface temperature in the tropics. *Journal of Climate*, *6*(10), 1898–1913.

References From the Supporting Information

Di Lorenzo, E., Schneider, N., Cobb, K. M., Franks, P. J. S., Chhak, K., Miller, A. J., et al. (2008). North Pacific Gyre Oscillation links ocean climate and ecosystem change. *Geophysical Research Letters*, *35*(8). https://doi.org/10.1029/2007GL032838

Nigam, S., Sengupta, A., & Ruiz-Barradas, A. (2020). Atlantic–Pacific links in observed multidecadal SST variability: Is the Atlantic multidecadal oscillation's phase reversal orchestrated by the pacific decadal oscillation? *Journal of Climate*, *33*(13), 5479–5505.

Xue, Y., Leetmaa, A., & Ji, M. (2000). ENSO prediction with Markov models: The impact of sea level. *Journal of Climate*, *13*(4), 849–871.

Geophysical Research Letters

Supporting Information for

Evolution of Subtropical Pacific-Onset El Niño: How its Onset Location Controls its Decay Evolution

Ji-Won Kim[1] and Jin-Yi Yu[1]

[1]Department of Earth System Science, University of California, Irvine, CA, USA

Contents of this file

Text S1. A method to calculate the SP- and TP-onset indices

We applied multivariate empirical orthogonal function (MEOF) analysis to calculate the Subtropical Pacific (SP)-onset index and the Tropical Pacific (TP)-onset index. An MEOF analysis is a statistical method that can identify the dominant coupled processes between multiple variables (cf. Xue et al., 2000; Yu & Fang, 2018, hereafter YF18). We applied it to capture the co-variability of ocean-atmosphere coupled processes associated with ENSO, which are manifested by the combined anomalies of SST, surface wind, and SSH over the tropical Pacific basin (i.e., 20°S to 20°N and 120°E to 70°W). Instead of the two-step MEOF as in YF18, we here simply used a one-step MEOF by taking input data of the combined anomalies as one block, e.g., $X(\vec{x}, t) = [\vec{x}^{SST}(t), \vec{x}^{wind}(t), \vec{x}^{SSH}(t)]$, where $\vec{x}$ is a spatial state vector for the incorporated variables and t is a time interval. All the input anomalies that have different units were standardized using a correlation matrix and smoothed by a three-month running mean filter in order to remove intraseasonal variability over the tropical Pacific, such as Madden–Julian Oscillation. The first three MEOFs from the observational data yield the leading coupled modes associated with ENSO, following YF18: one is the ENSO mature mode (as 1st MEOF) and the others are the ENSO onset modes (as 2nd and 3rd MEOFs). The 2nd MEOF mode represents the SP-onset mechanism characterized by positive SST anomalies extending from the tropical central Pacific into the subtropical North Pacific, with accompanying positive SSH and westerly wind anomalies there. The 3rd MEOF mode corresponds to the TP-onset mechanism characterized by a narrow belt of positive SST anomalies on the eastern equatorial Pacific, with accompanying positive SSH and westerly wind anomalies along the entire equatorial Pacific (note that readers can find the classical spatiotemporal patterns associated with the three MEOF modes in YF18). As a consequence, the principal components of 2nd and 3rd MEOF modes are respectively the SP- and TP-onset indices. The same MEOF analysis was applied to the 2,200-yr CESM1 simulation utilized in this study.

The SP-onset index here has interannual and decadal variations in both the observations and model simulation (figures not shown). This indicates that the SP-onset index likely has contributions from variability in the interannual and decadal timescales. Hence, we add a caveat to state that the SP-onset index may interplay with other Pacific decadal variability modes such as the North Pacific Gyre Oscillation (Di Lorenzo et al., 2008) or the Pan-Pacific decadal variability (Nigam et al., 2020).

Text S2. The IOD and PMM indices

Aside from the Niño3.4 index, two other climate indices were also used in this study: the Indian Ocean Dipole (IOD) index and the Pacific Meridional Mode (PMM) index. The IOD index represents a dipole/zonal SSTA mode in the Indian Ocean basin that has a prominent inter-annual variability. It is defined as the normalized SSTA difference between the western Indian Ocean (10°S–10°N and 50–70°E) and the southeastern Indian Ocean (10°S to the equator and 90–110°E) during boreal fall from September to November,

in which IOD events usually peak (Saji et al., 1999). The PMM index represents the coupled SST–surface wind pattern over the subtropical northeastern Pacific. It is defined as the normalized SSTA over the PMM region in the North Pacific (15–25°N and 150–120°W; cf. Amaya, 2019) during boreal spring from March to May, in which PMM events usually peak (Chiang & Vimont, 2004).

Text S3. Role of the NTA SST warming in the decay evolutions of SP-onset El Niños

Previous studies suggested that El Niños can lead to the SST warming over the north tropical Atlantic (NTA) during boreal spring after they peaks via the El Niño-associated atmospheric teleconnection pattern (e.g., Enfield & Mayer, 1997; Saravanan & Chang, 2000). This El Niño-induced NTA warming can subsequently trigger a cold event in the subsequent winter by inducing western Pacific easterlies (which is known as the transitioning effect of the NTA SST warming on ENSO evolution; cf. Ham et al., 2013; Wang et al., 2017). Therefore, it may be possible that the NTA warming also has a potential role in affecting the decay evolutions of SP-onset El Niños. In response, we first checked if there is an El Niño-induced SST warming over the NTA during boreal spring after the SP-onset El Niños peak. Here we utilized two groups of SP-onset El Niños classified in this study: Group-A (eastward onset and cyclic evolution events) and Group-B (westward onset and multiyear evolution events). As shown in Fig. S7a and S7b, the Group-A and Group-B events both show positive SSTAs over the NTA during their decaying spring (i.e., March^{+1}–May^{+1}), indicating the existence of El Niño-induced NTA SST warming. The intensity of NTA SST warming is detected as being slightly stronger in Group-A than Group-B (cf. Fig. S7a and S7b). This suggests the possibility that the cyclic evolution of Group-A events can also be affected by the transitioning effect of the NTA SST warming, in addition to that of the positive IOD in this study. For this reason, we further checked the NTA SST warming intensities by calculating the SSTA averaged over the NTA region (i.e., 5–25°N and 75–15°W; green boxes in Fig. S7) to see if the intensities are clearly different between the two groups. The result displayed in Fig. S7c, however, shows that the NTA SST warming intensities are quite comparable between Group-A (~0.28°C) and Group-B (~0.21°C) with no statistically significant difference. Thus, based on the results, the abovementioned suggestion cannot be firmly asserted. Sophisticated numerical experiments are highly needed to identify whether the NTA SST warming plays any role in controlling the decay evolutions of SP-onset El Niños.

Table S1. Classification of observed El Niños during 1958–2019 into SP-, TP-, and Mixed-onset events by comparing the SP-onset index in the preceding spring (i.e., March^0–May^0) and the TP-onset index in the preceding summer (i.e., June^0–August^0) (see Sect. 3.1 for details). Their evolution patterns of either cyclic or multiyear are shown in the rightmost column. Note that the rows of SP-, TP-, and mixed-onset El Niños are expressed as red, blue, and green colors, respectively. The remaining El Niños that are classified as neither SP-, TP-, nor mixed-onset events are notated as N/A (i.e., not applicable) in the 4th column. These events are not able to determine their dominant onset mechanisms based on the TP- and SP-onset indices alone.

El Niño year	SP-onset index in the preceding spring	TP-onset index in the preceding summer	Dominant onset mechanism	Evolution pattern
1958-1959	-0.70	-1.15	N/A	Cyclic
1963-1964	1.49	0.64	SP-onset	Cyclic
1965-1966	-0.83	1.35	TP-onset	Cyclic
1968-1969	1.28	0.09	SP-onset	Multiyear
1969-1970	-0.05	-0.81	N/A	Cyclic
1972-1973	0.58	2.11	TP-onset	Cyclic
1976-1977	0.06	2.20	TP-onset	Multiyear
1977-1978	-1.00	0.24	N/A	Multiyear
1979-1980	-0.58	0.46	N/A	Cyclic
1982-1983	0.70	1.96	TP-onset	Cyclic
1986-1987	0.56	1.01	Mixed-onset	Multiyear
1987-1988	-1.06	0.74	TP-onset	Cyclic
1991-1992	0.50	0.70	Mixed-onset	Multiyear
1994-1995	1.21	0.46	SP-onset	Cyclic
1997-1998	1.02	2.56	TP-onset	Cyclic
2002-2003	0.79	0.67	Mixed-onset	Multiyear
2004-2005	0.97	0.31	SP-onset	Cyclic
2006-2007	0.01	0.52	TP-onset	Cyclic
2009-2010	0.15	0.52	Mixed-onset	Cyclic
2014-2015	0.93	0.40	SP-onset	Multiyear
2015-2016	1.74	2.11	Mixed-onset	Cyclic
2018-2019	1.88	0.45	SP-onset	Multiyear

Table S2. Statistical properties of the SP- and TP-onset El Niños identified in the CESM1 simulation. Values in parentheses are percentages calculated from the total number of events. Note that the rows of SP- and TP-onset El Niños are expressed as red and blue, respectively.

Dominant onset mechanism	Total number of events	Number of cyclic evolution events	Number of multiyear evolution events
SP-onset	139	71 (51.1%)	68 (48.9%)
TP-onset	155	108 (69.6%)	47 (30.3%)

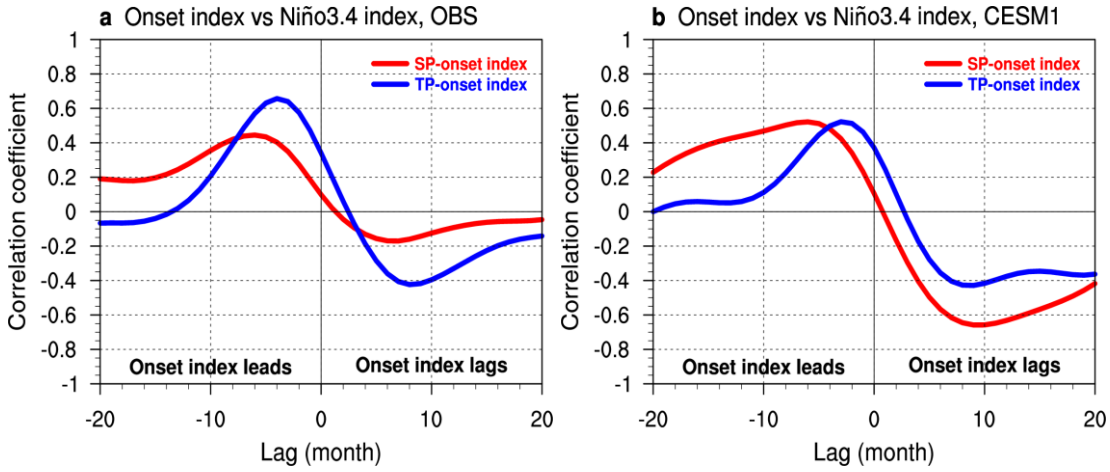

Figure S1. Lead-lag correlations between the SP- (red curve) or TP-onset (blue curve) index and the Niño3.4 index in (a) the observations and (b) the CESM1 simulation. In both the observations and the CESM1 simulation, the SP-onset index has a longer lead time when leading the Niño3.4 index than the TP-onset index does. This implies that the SP-onset El Niños begin earlier than the TP-onset El Niños, which is consistent with the result from YF18.

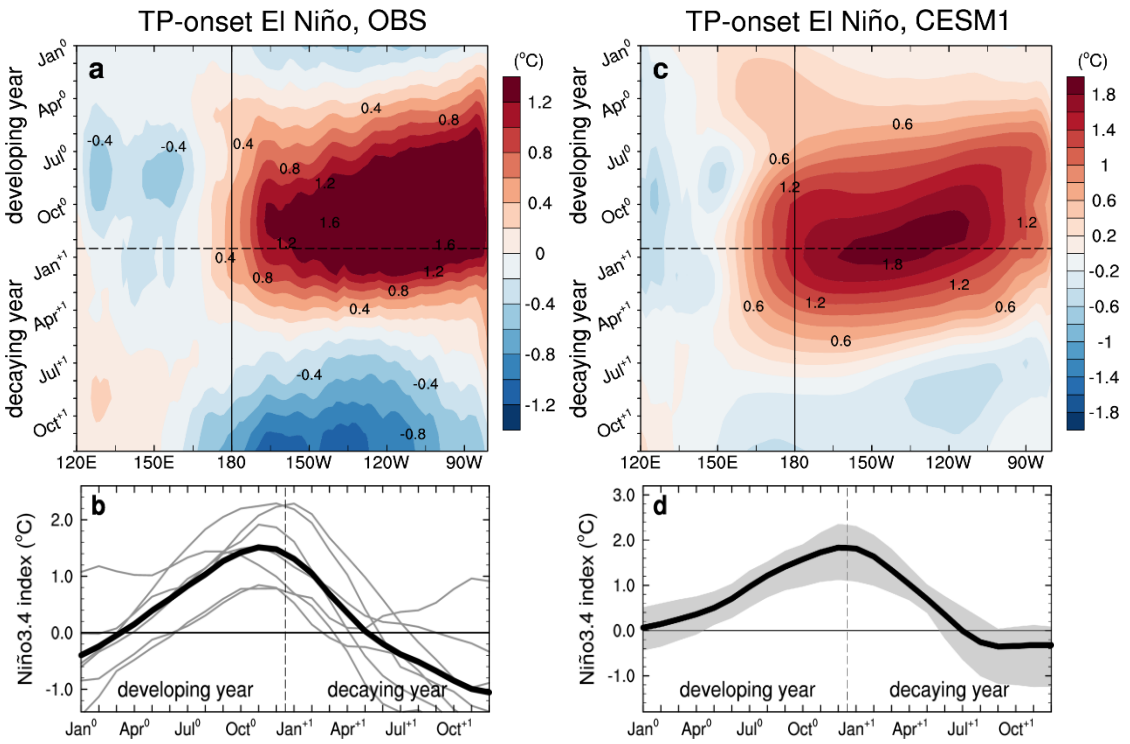

Figure S2. Composite structures and evolutions of TP-onset El Niños. (a, b) Longitude-time plot of equatorial (i.e., 5°S–5°N) SSTAs during the developing and decaying years from January^{0} to December^{+1} for the observations is presented in the upper panel. Temporal evolution of the Niño3.4 index during the developing and decaying years in the observations is presented in the lower panel. The gray curves in (b) indicate individual event evolutions. (c, d) are the same as (a, b) except for the CESM1 simulation and the gray shading in (d) indicates interquartile ranges between the 25th and 75th percentiles.

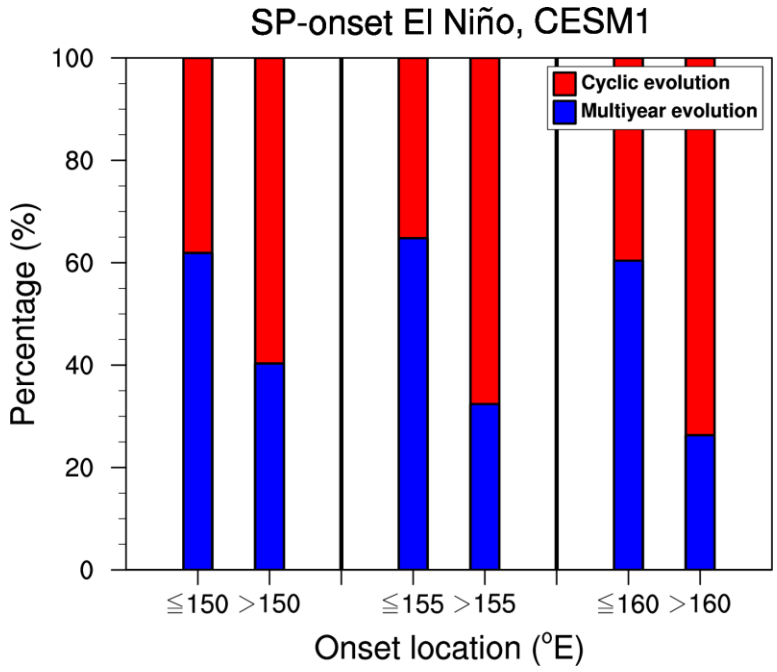

Figure S3. *Left* Percentages of SP-onset El Niños in the CESM1 simulation that have either cyclic (red bar-chart) or multiyear (blue bar-chart) evolution when the onset location is situated to the west and east of the criterion longitude, 150°E. *Middle* and *right* panels are the same as the *left* except for the criterion longitudes of 155°E and 160°E, respectively.

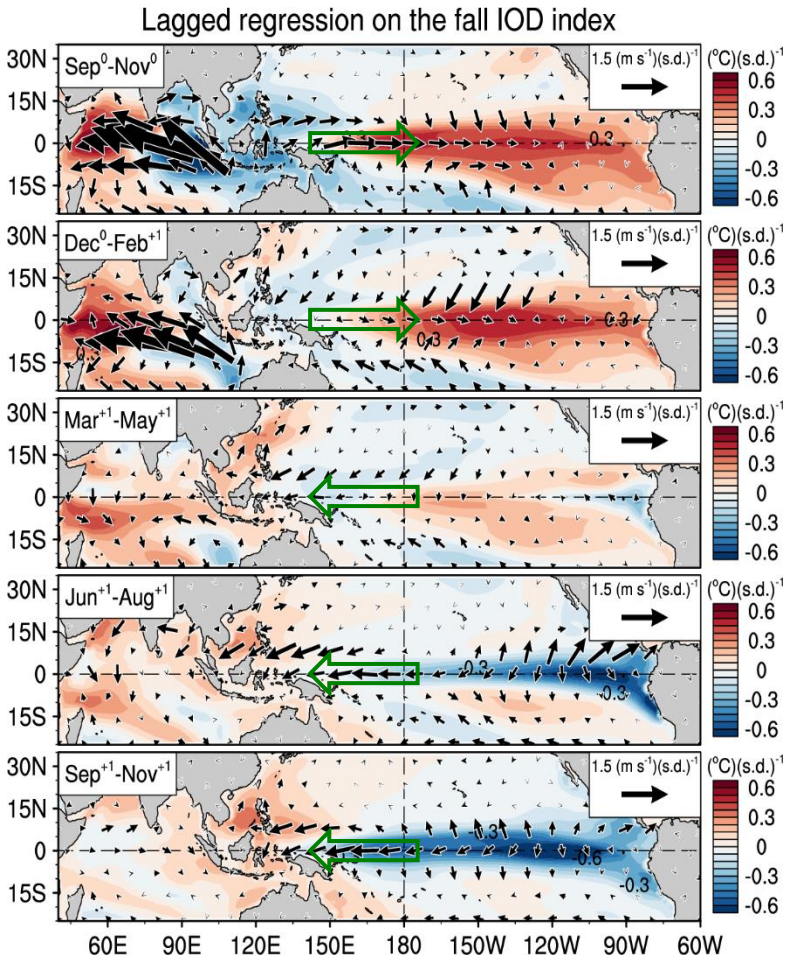

Figure S4. The transitioning effect of a positive IOD on El Niño evolution. Lagged regression maps on the fall (i.e., September^{0}–November^{0}) IOD index using anomalous SST (shadings) and surface wind (vectors) during seasons from the first fall of September^{0}–November^{0} to the second fall of September^{+1}–November^{+1}. The effect of PMM has been excluded by computing partial regression coefficients of the IOD index with respect to the PMM index. The green arrows indicate the zonal directions of surface wind anomalies over the tropical western Pacific, which change from westerly anomalies during fall and winter to easterly anomalies in the following seasons.

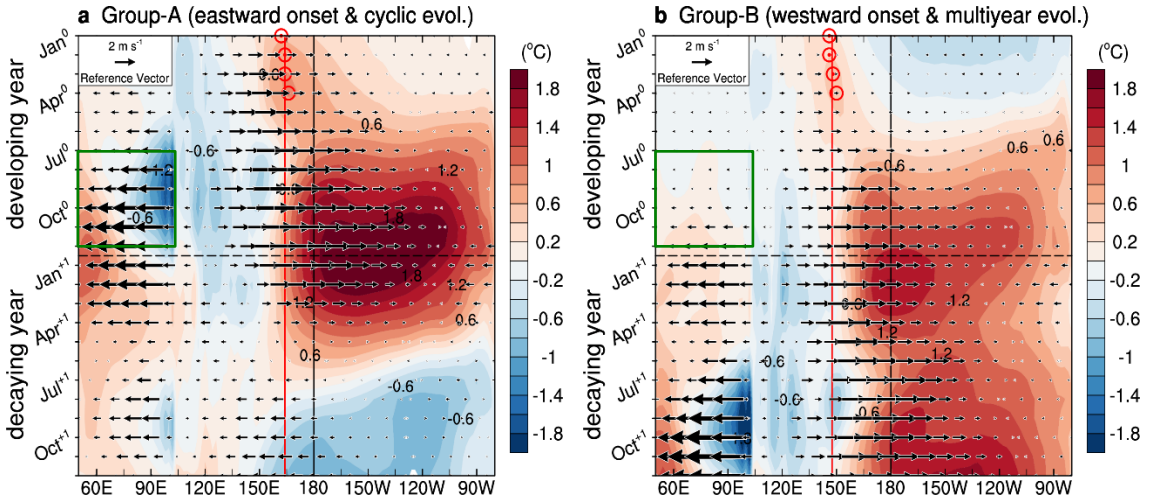

Figure S5. Longitude-time plot of composite anomalous SST (shadings; in °C) and zonal wind (vectors; in m s^{-1}) averaged over the equator (i.e., 5°S to 5°N) during the developing and decaying years from January^{0} to December^{+1} for the events of (a) Group-A and (b) Group-B. In figure, the red circled dots mark the maximum warm SSTAs from January^{0} to April^{0} and the red vertical lines denote their averaged longitudinal positions. The green rectangular areas indicate a phase of the IOD in the Indian Ocean, with a strong positive IOD for the Group-A events and a neutral IOD for the Group-B events.

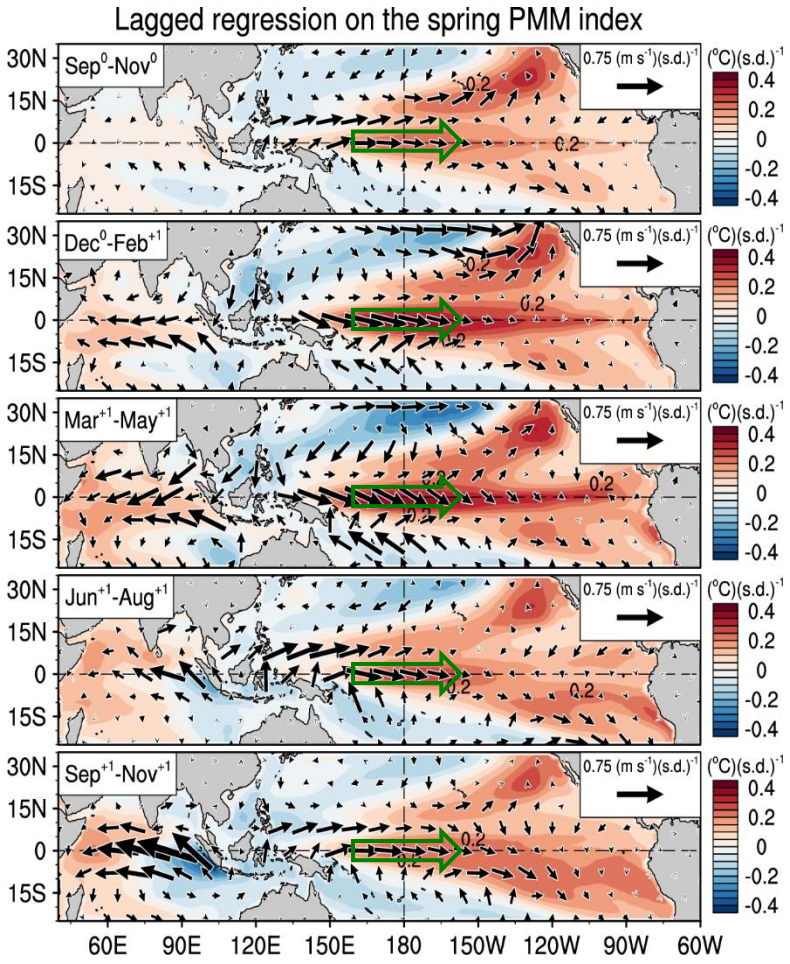

Figure S6. The lingering effect of a positive PMM on El Niño evolution. Lagged regression maps on the spring (i.e., March^{+1}–May^{+1}) PMM index using anomalous SST (shadings) and surface wind (vectors) during seasons from the first fall of September^{0}–November^{0} to the second fall of September^{+1}–November^{+1}. The effect of IOD has been excluded by computing partial regression coefficients of the PMM index with respect to the IOD index. The green arrows indicate the prevailing westerly wind anomalies over the central equatorial Pacific which persist throughout seasons.

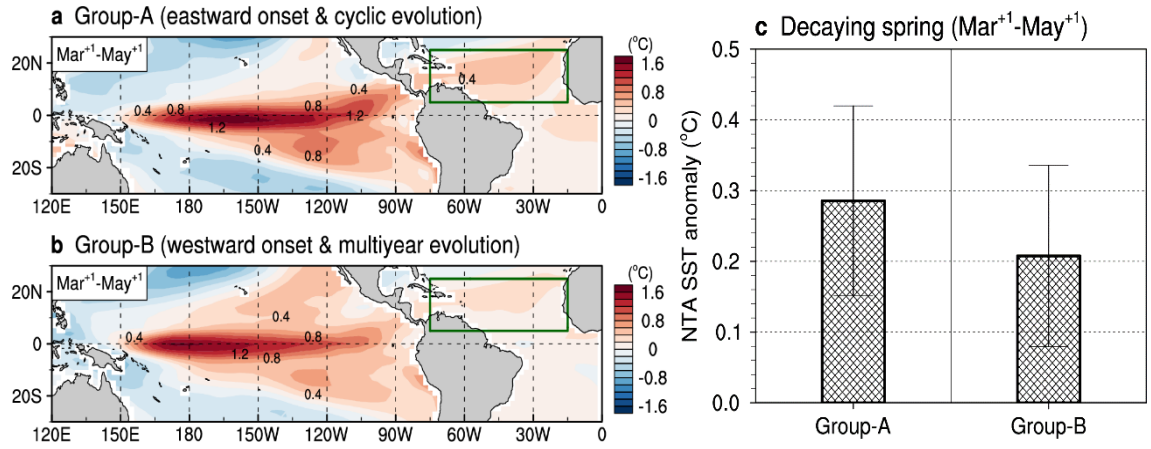

Figure S7. Composite structures of anomalous SST (in °C) over the tropical Pacific and Atlantic Oceans during the decaying spring (i.e., March^{+1}–May^{+1}) for the (a) Group-A and (b) Group-B events. The green boxes denote an area for the north tropical Atlantic (NTA) region (i.e., 5–25°N and 75–15°W). (c) Mean intensity of SSTA averaged over the NTA during the decaying spring for Group-A (left panel) and Group-B (right panel). Error bars represent 1 standard deviation about the mean.

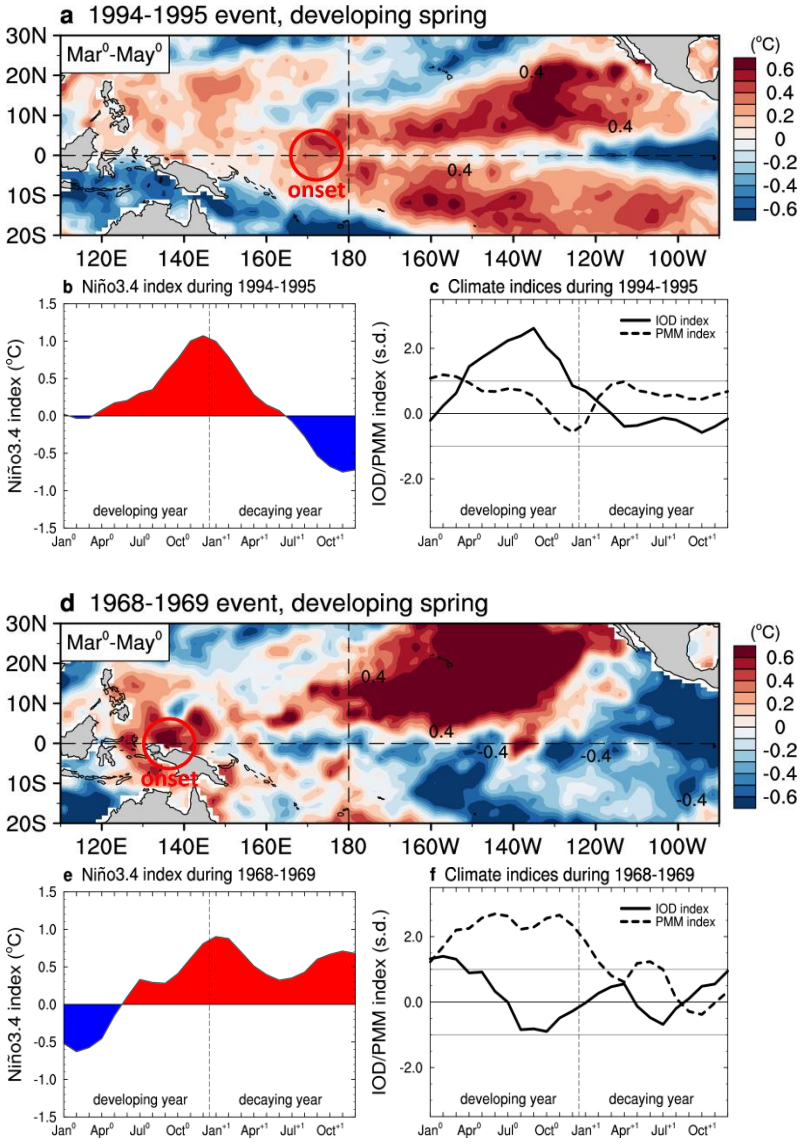

Figure S8. (a) Spatial structure of anomalous SST (in °C) during the developing spring (i.e., March^{0}–May^{0}) of the 1994–1995 SP-onset El Niño event. The red circle denotes the center of onset location for the event. (b) Temporal evolution of the Niño3.4 index (shadings; in °C) during the developing and decaying years (i.e., January^{0}–December^{+1}) for the event. (c) Same as (b) but for the IOD (solid curve; in s.d.) and PMM (dashed curve; in s.d.) indices. (d-f) are the same as (a-c) except for the 1968–1969 SP-onset El Niño event.

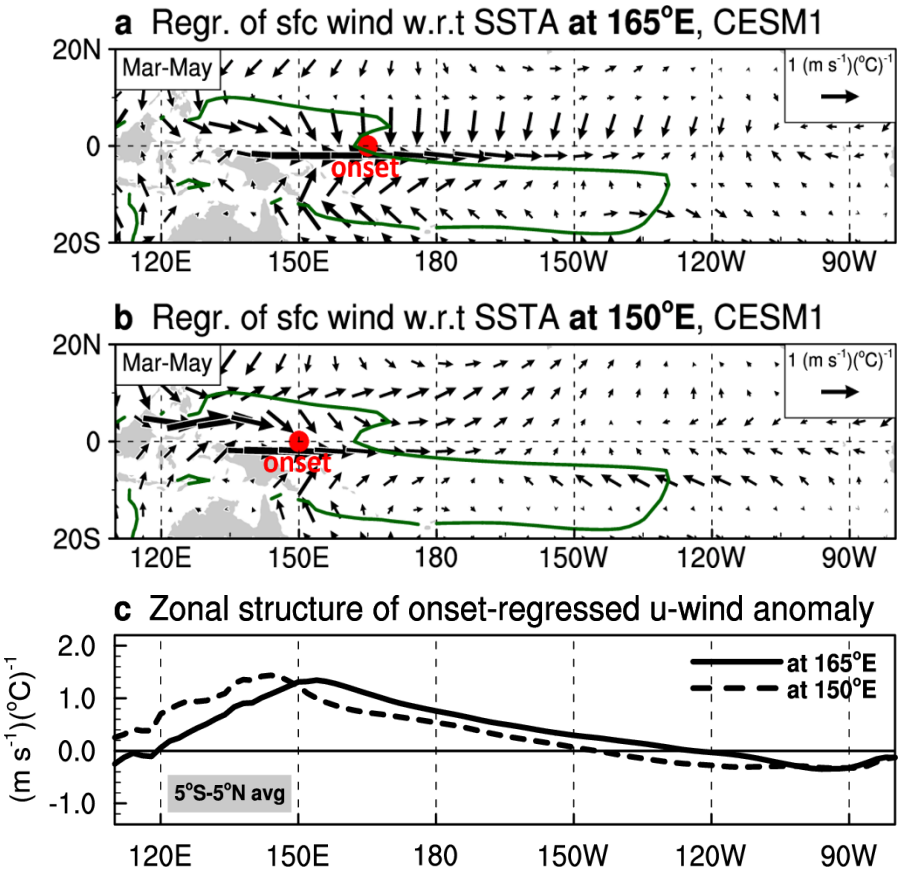

Figure S9. Regression maps of anomalous surface wind during boreal spring (i.e., March–May) onto the one-point SST anomaly located at (a) 165°E and (b) 150°E on the equator in the CESM1 simulation (namely, the onset). The onset locations are marked as red dots and the green contours denote climatological 28°C isotherm line which depicts an area for the western Pacific warm pool. The onset is on the eastern edge of the warm pool when the onset is located at 165°E, while the onset is inside the warm pool when the onset is located at 150°E (representing the onset locations of Group-A and Group-B events). (c) Zonal structure of the onset-regressed zonal wind anomaly averaged over 5°S–5°N for the onset located at 165°E (solid curve) and 150°E (dashed curve)

Reference

Amaya, D. J. (2019). The Pacific meridional mode and ENSO: A review. *Current Climate Change Reports*, *5*(4), 296-307.

Chiang, J. C., & Vimont, D. J. (2004). Analogous Pacific and Atlantic meridional modes of tropical atmosphere–ocean variability. *Journal of Climate*, *17*(21), 4143-4158.

Di Lorenzo, E., Schneider, N., Cobb, K. M., Franks, P. J. S., Chhak, K., Miller, A. J., ... & Powell, T. M. (2008). North Pacific Gyre Oscillation links ocean climate and ecosystem change. *Geophysical Research Letters*, *35*(8).

Enfield, D. B., & Mayer, D. A. (1997). Tropical Atlantic sea surface temperature variability and its relation to El Niño-Southern Oscillation. *Journal of Geophysical Research: Oceans*, *102*(C1), 929-945.

Ham, Y. G., Kug, J. S., Park, J. Y., & Jin, F. F. (2013). Sea surface temperature in the north tropical Atlantic as a trigger for El Niño/Southern Oscillation events. *Nature Geoscience*, *6*(2), 112-116.

Nigam, S., Sengupta, A., & Ruiz-Barradas, A. (2020). Atlantic–Pacific Links in Observed Multidecadal SST Variability: Is the Atlantic Multidecadal Oscillation's Phase Reversal Orchestrated by the Pacific Decadal Oscillation?. *Journal of Climate*, *33*(13), 5479-5505.

Saji, N. H., Goswami, B. N., Vinayachandran, P. N., & Yamagata, T. (1999). A dipole mode in the tropical Indian Ocean. *Nature*, *401*(6751), 360.

Saravanan, R., & Chang, P. (2000). Interaction between tropical Atlantic variability and El Niño–Southern oscillation. *Journal of climate*, *13*(13), 2177-2194.

Wang, L., Yu, J. Y., & Paek, H. (2017). Enhanced biennial variability in the Pacific due to Atlantic capacitor effect. *Nature communications*, *8*(1), 1-7.

Xue, Y., Leetmaa, A., & Ji, M. (2000). ENSO prediction with Markov models: The impact of sea level. *Journal of Climate*, *13*(4), 849–871.

Yu, J. Y., & Fang, S. W. (2018). The Distinct Contributions of the Seasonal Footprinting and Charged-Discharged Mechanisms to ENSO Complexity. *Geophysical Research Letters*, *45*(13), 6611-6618.